Multilayer relaxation of the Al(210) surface

D. L. Adams, V. Jensen, X. F. Sun,* and J. H. Vollesen
Institute of Physics, University of Aarhus, DK-8000 Aarhus C, Denmark
(Received 18 April 1988)

The surface structure of Al(210) has been determined by means of a systematic minimization of the discrepancy between experimental low-energy electron diffraction intensity-energy spectra and spectra calculated using multiple-scattering theory, as a function of the structural and nonstructural variables of the calculations. The experimental data base consists of intensity-energy spectra for 14 symmetry-inequivalent diffracted beams, measured at normal incidence and at 135 K in the energy range 40–340 eV. The surface structure is found to exhibit an oscillatory, multilayer relaxation. The relaxations Δd_i and Δr_i of the first five interlayer spacings and registries with respect to the corresponding bulk values are determined to be $\Delta d_1 = -(16\pm2)\%$, $\Delta d_2 = -(1\pm3)\%$, $\Delta d_3 = +(9\pm3)\%$, $\Delta d_4 = -(4\pm4)\%$, $\Delta d_5 = -(1\pm5)\%$, and $\Delta r_1 = (0\pm3)\%$, $\Delta r_2 = -(3\pm3)\%$, $\Delta r_3 = +(2\pm3)\%$, $\Delta r_4 = -(2\pm4)\%$, $\Delta r_5 = -(1\pm5)\%$. These results are in qualitative agreement with the results of pseudopotential calculations of the surface structure of Al(210) by Barnett, Landman, and Cleveland [Phys. Rev. Lett. **51**, 1359 (1983)] in the sense that the signs of the relaxations, where + indicates an expansion and − a contraction, are the same for each of the relaxations. Furthermore, the present results are in near-quantitative agreement with the relaxations calculated by Jiang, Marcus, and Jona [Solid State Commun. **59**, 275 (1986)] and F. Jona (private communication), using a simple electrostatic, point-ion–frozen-background model. The present results for Al(210) are discussed in the context of previous experimental studies of the multilayer relaxation of open metal surfaces, which are reviewed with a view to the identification of trends in the observed phenomena. In particular, the relaxation behavior of the first six surfaces of Al and Fe are discussed in the framework of the point-ion–frozen-background model. It is demonstrated that the relaxation trends can be predicted by simple considerations of the electrostatic forces on the layers of the unrelaxed surface structures, thus providing the basis for a simple, intuitive description of multilayer relaxation.

I. INTRODUCTION

Recent studies of the structure of open metal surfaces have revealed the existence of relaxation phenomena extending several layers into the solid. The study of this phenomenon has proved to be a useful testing ground for the refinement of experimental methods of structure determination and for the development of quantitative theories of surface electronic and geometrical structure. The work described in this article was carried out with a view to providing further impetus to these developments and, in particular, to test the recent prediction for the surface structure of Al(210) resulting from the calculations of Barnett, Landman, and Cleveland.[1] To anticipate the conclusions presented in more detail later, the trends of the relaxation behavior found in the present experimental low-energy electron diffraction (LEED) study are in remarkable agreement with the predicted trends, but the magnitude of the relaxations is generally smaller than predicted.

Although the present work is limited to the consideration of unreconstructed surface structures of elemental metals, it should be noted that the occurrence of significant relaxation effects is not limited to such relatively simple systems. A few, very recent studies of alloy surfaces,[2] reconstructed metal surfaces,[3] and adsorption systems[4] suggest that multilayer relaxation phenomena may be of general importance for open surfaces.

Previous work on the relaxation of unreconstructed metal surfaces is reviewed in Sec. II. The structure of an ideal Al(210) surface is described in Sec. III. The experimental and calculational LEED procedures used in the present work are described in Secs. IV and V, respectively. The *r*-factor procedures used in the comparison of experimental and calculated LEED intensity-energy spectra are discussed in Sec. VI, and their application to the determination of the surface structure of Al(210) is described in Sec. VII. Finally, in Sec. VIII, the present results are compared with theoretical predictions of the surface structure of Al(210), and placed in the context of previous studies of multilayer relaxation. Trends in the relaxation of Al and Fe surfaces are identified and discussed in the framework of effective-medium and point-ion models. It is demonstrated that an intuitive understanding of multilayer relaxation can be achieved through consideration of the electrostatic forces on the ions of the unrelaxed surface structure.

II. PREVIOUS STUDIES OF THE RELAXATION OF UNRECONSTRUCTED METAL SURFACES

A. Relaxation of the first interlayer spacing

The first determination of a significant deviation from the geometry of an ideal, truncated-bulk crystal was made, for Al(110), in the pioneering LEED study of Jep-

sen, Marcus, and Jona[5] in 1972. In one of the first quantitative applications of LEED to the determination of surface structure, these authors found a contraction of the spacing between the first two layers of the Al(110) surface of $\Delta d_1 = -10\%$ with respect to the bulk value. In contrast, the Al(111) and (100) surfaces were found to correspond to almost perfect truncations of a bulk crystal, with $\Delta d_1 = +2.5\%$ and 0%, respectively. Subsequent LEED studies have indicated that a contraction of the first interlayer spacing occurs quite generally for open metal surfaces, whereas the close-packed fcc (111) and (100), bcc (110), and hcp (0001) surfaces are essentially unrelaxed. The magnitude of the relaxation increases generally with surface roughness.

The occurrence of a contraction of the first interlayer spacing, as opposed to the expansion predicted in earlier pair-potential calculations,[6] can be understood in terms of the electrostatic interaction between point ions and a homogeneous electron charge distribution with a step termination at the surface.[7]

By considering only the interaction within a single Wigner-Seitz cell at the surface, Finnis and Heine[7] showed that the asymmetric charge distribution within the cell results in an inward-directed force on the ions in the first layer. Calculations based on this simple model for Al(111), (100), and (110) led to relaxations of the first interlayer spacing of $\Delta d_1 = -1.6\%$, -4.6%, and -16%, respectively, in qualitative agreement with the trends found in the LEED results of Jepsen *et al.*[5] At about the same time, a relaxation of the first interlayer spacing of Li(100) of $\Delta d_1 = -20\%$ was predicted by Alldredge and Kleinman.[8] In a more detailed study than that of Finnis and Heine, these authors showed that it was important to include the interactions between the surface Wigner-Seitz cells, and to include the effects of the full, three-dimensional variation of the electron charge density, the latter being taken from the results of a band-structure calculation.

Quantitative agreement between experimental and theoretical surface structures was not achieved, however, in the decade following the work of Jepsen *et al.*, except in the case of essentially unrelaxed surfaces.[9] Various calculations for Al(110), for example, gave results[10] scattered in the range $\Delta d_1 = -26\%$ to $+2\%$, as compared to the experimental value of -10%.

B. Multilayer relaxation of interlayer spacings

The possibility that the relaxation of metal surfaces might extend deeper into the solid appears to have been first examined in the context of experimental determination of surface structure by Davis and co-workers[11–13] in LEED studies of Cu(110) in 1978–1980. The conclusion of this work ($\Delta d_1 = -10\%$, $\Delta d_2 = 0\%$), however, was that only the first interlayer spacing was relaxed. More recently the improved precision of LEED analyses, resulting in part from the use of *r*-factor methods and systematic parameter variation, has led to the observation of multilayer relaxation for a number of systems, as discussed below.

The first detailed theoretical investigation of multilayer relaxation was reported by Landman, Hill, and Mostoller[14] in 1980 for the (111), (100), and (110) surfaces of Li, Na, Al, and Cu. Equilibrium surface structures were determined by iterative adjustment of the relative positions of planes of ions parallel to the surface to reduce the net electrostatic forces on the ions to zero. The electrostatic forces due to the mutual interaction of the ions and their interaction with the valence electrons were calculated by the planar summation method used by Alldredge and Kleinman.[8] The influence of various ionic pseudopotentials and various one-dimensional variations of the electron charge density on the equilibrium surface structures was investigated, but no self-consistent adjustment of the electron charge density was carried out in the iterative procedure.

The trends of the relaxations of the first interlayer spacings calculated by Landman *et al.* were consistent with the trends found in experimental studies, referred to previously, except for the bcc (111) surfaces where expansions of the first interlayer spacing were predicted. A novel feature of the results was the prediction of substantial relaxations of deeper interlayer spacings for the fcc (110) and bcc (100) surfaces. The relaxations were found to oscillate in sign from $-$ to $+$ and to be damped in magnitude in the direction of the bulk, that is, a contraction of the first interlayer spacing is followed by a smaller expansion of the second interlayer spacing, which is followed in turn by a smaller contraction of the third interlayer spacing, and so on. The magnitude of the relaxations was found to depend strongly on the particular ingredients of the model calculations, but the qualitative trends were given in all cases by the most simple model assumptions, involving the interaction of point ions with a step-terminated, homogeneous electron charge density.

The qualitative trends of the multilayer relaxations predicted by Landman *et al.* were subsequently confirmed by LEED and high-energy ion-scattering (HEIS) studies carried out in our laboratory for Cu(110) (Refs. 15–17) and Al(110).[10,18] However, the magnitude of the relaxations, as listed together with the predicted values in Table I, was found to be smaller and more rapidly damped into the bulk than predicted. For Cu(110), the near-quantitative agreement between the results obtained by LEED and HEIS gave some confidence in the reality of the small relaxation of the second interlayer spacing. Subsequent LEED (Refs. 19 and 20) and HEIS (Ref. 21) studies, with results also listed in the table, have substantiated our original findings.

More recently, the inclusion of self-consistency conditions at various levels of sophistication in calculations of surface structure[22–24] has led to quantitative agreement with the relaxations determined by LEED for Al(110) (Refs. 10 and 18) and V(100).[25] A comparison of the results calculated by Barnett, Landman, and Cleveland[22] and by Ho and Bohnen[24] for Al(110) with the experimental LEED results is given in Table II.

Following the studies of Cu and Al(110) discussed above, damped, oscillatory relaxation of the interlayer spacings has been reported for V (Ref. 25) and Ta(100),[26] Ni,[27–31] Ag,[32,33] Pb (Ref. 34) and Pd(110),[35] Ni (Ref. 36) and Al(311),[37] Fe(211),[38] and Fe(310).[39] Both LEED and

TABLE I. Comparison of experimental and (non-self-consistent) theoretical surface structures for Cu and Al(110).

Surface	Relaxations (%) Δd_1	Δd_2	Δd_3	Method
Cu(110)				
Theory	−26.3	+ 15.8[a]		
Experiment	−10	0[b]		LEED
	−8.5	+ 2.3[c]		LEED
	−7.9	+ 2.4[d]		LEED
	−10.0	+ 1.9[d]		LEED
	−5.3	+ 3.3[e]		HEIS
	−7.5	+ 2.5[f]		HEIS
Al(110)				
Theory	−21.3	+ 13.3	−6.7[g]	
Experiment	−8.6	+ 5.0	−1.6[h]	LEED
	−8.5	+ 5.5	+ 2.2[i]	LEED

[a]Reference 14. Step density profile.
[b]Reference 12.
[c]References 15 and 17.
[d]Reference 19.
[e]References 15 and 16.
[f]Reference 21.
[g]Reference 14. Exponential density profile.
[h]References 10 and 18.
[i]Reference 20.

HEIS determinations have been made in the case of Ni and Ag(110). For all of these surfaces, the signs of the relaxations are $-+-$. More complex relaxation behavior has been found for Fe(111) (Ref. 40) and (210) (Ref. 41) and for Al(331) (Ref. 42) where the signs of the relaxations are $--+-$. In addition, the magnitude of the relaxations of the Fe(210) and Al(331) surfaces are damped in a nonuniform fashion into the bulk. In both cases, the expansion of the third interlayer spacing is larger than the contraction of the second interlayer spacing.

C. Multilayer relaxation of interlayer registries

The recent LEED results of Solokov *et al.*[38,39,41] for Fe(211), (310), and (210) revealed the occurrence of a new relaxation phenomena, in that relaxation of the interlayer spacings was found to be accompanied by substantial relaxation of the interlayer registries. It can be noted that for these more open surfaces, the surface space group of the ideal structure contains a single mirror plane. Relative displacements of layers parallel to the surface in the surface mirror-line direction can occur, therefore, without loss of symmetry.

TABLE II. Comparison of experimental and (self-consistent) theoretical surface structures for Al(110).

	Relaxations (%) Δd_1	Δd_2	Δd_3
Theory	−10	+ 4	−3[a]
	−6.8	+ 3.5	−2.0[b]
Experiment	−8.6	+ 5.0	−1.6[c]
	−8.5	+ 5.5	+ 2.2[d]

[a]Reference 22.
[b]Reference 24.
[c]References 10 and 18.
[d]Reference 20.

At about the same time as the work of Solokov *et al.*, Barnett *et al.*[1] reported calculations for the (210) and (211) surfaces of Al and Na which also showed the occurrence of substantial relaxations of both the interlayer spacings and registries. The model used was essentially that of Landman *et al.*[14] for calculating the electrostatic interactions between a lattice of ionic pseudopotentials and a one-dimensional, Lang-Kohn,[9] electron density profile, and did not include the self-consistent screening corrections made in the calculations by the same authors for Al(110).

The experimental LEED results for Fe(211) and (210) are listed together with the calculated results for Na(211) and (210) in Table III, from which it can be seen that the qualitative trends are similar, except for the signs of the second and third interlayer registries in the case of the bcc (210) surfaces.

The extent to which the differences in magnitude between the experimental and calculated relaxations reflect the differences in the electronic structure of Na and Fe, or result as in the case of Al(110) from the lack of self-consistency in the calculations is an open question. A main purpose of the present work was to make a direct comparison with the corresponding calculations of Barnett *et al.*, for Al(210).

Finally, it is noted that experimental reports of substantial relaxations of interlayer registries are limited to the Fe(211), (310), and (210) surfaces. A small relaxation of the first interlayer registry was found for Al(331), but the other fcc metal surfaces containing a single mirror plane which have been studied to date, namely Ni and Al(311), exhibit essentially no relaxation of the interlayer registries.

TABLE III. Comparison of experimental (Fe) and calculated (Na) relaxations for bcc (21) and (210) surfaces.

Relaxation	Fe(211)	Na(211)	Fe(210)	Na(210)
Δd_1	−10.4	−21.1	−22.0	−41.1
Δd_2	+5.4	+16.0	−11.1	−65.4
Δd_3	−1.3	−11.1	+17.0	+88.3
Δd_4		+7.6	−4.8	−31.2
Δr_1 [a]	+29.0	+32.4	+7.1	+13.3
Δr_2	−4.5	−35.7	+1.4	−2.3
Δr_3		+16.8	0.0	−13.7
Δr_4		−3.8	+4.0	+7.0

[a] Δr_i is the percentage change of the component lying in the surface mirror line of the *shortest* vector connecting atoms in the ith and $(i+1)$th layers, with respect to the corresponding bulk value.

III. STRUCTURAL INPUT AND NOMENCLATURE

Sketches of the atomic arrangement in an ideal fcc (210) surface[43] are shown in Fig. 1. The (210) plane is the sixth most close-packed plane in the fcc structure, with unit-cell area 2.58 times larger than that of the most close-packed (111) plane.

As indicated in Fig. 1(a), the surface structure can be specified by primitive unit mesh vectors, $\mathbf{a}_1$ and $\mathbf{a}_2$, and by an interlayer shift vector $\mathbf{s}$ which connects origins in successive layers. The surface-normal component of $\mathbf{s}$ is referred to as the interlayer spacing d, and the surface-parallel component of $\mathbf{s}$ lying in the $[1\bar{2}0]$ mirror-line direction is referred to as the interlayer registry r.

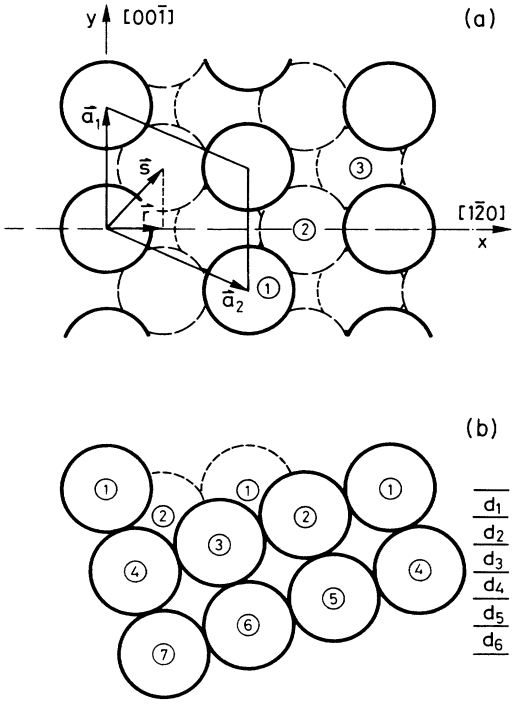

FIG. 1. Hard-sphere model of the ideal fcc (210) surface. (a) Projection on the (210) plane (top view). Atoms in the first layer are shown by solid circles. Atoms in the second and third layers are shown by dashed circles. The primitive unit mesh is defined by the vectors $\mathbf{a}_1$ and $\mathbf{a}_2$. The interlayer shift vector $\mathbf{s}$ connects origins in successive planes. The interlayer registry r is the projection of $\mathbf{s}$ on the $[1\bar{2}0]$ mirror line. (b) Projection on the (001) plane (side view). Atoms lying in the same (001) plane are shown by solid circles. The interlayer spacings d_i are indicated.

It is noted that alternative specifications of the interlayer shift vector $\mathbf{s}$ lead to different specifications of the interlayer registry r. Thus the description of a possible relaxation of r as being a contraction or expansion, and the percentage change Δr with respect to the bulk value, depend upon the choice of $\mathbf{s}$. In discussing the results of previous studies of the relaxation of interlayer registries we have, where necessary, recalculated the results in accordance with the definition of $\mathbf{s}$ used here as the *shortest* vector connecting atoms in successive layers.

As described in Sec. IV, experimental LEED measurements for Al(210) exhibit the full surface space-group symmetry of an ideal fcc (210) surface, including the mirror-plane symmetry. Thus the possible relaxations of the interlayer shift vector $\mathbf{s}_i$ connecting origins in the ith and $(i+1)$th layers are restricted to relaxations Δd_i and Δr_i lying in the (001) plane [Fig. 1(b)]. The bulk values of s, d, and r are $s=a_0/\sqrt{2}=2.8543$ Å, $d=\sqrt{5}a_0/10=0.9026$ Å, and $r=\sqrt{5}a_0/5=1.8052$ Å, based on the value of the lattice constant $a_0^{135}=4.036\,57$ Å at 135 K, as derived from the value[44] at room temperature of $a_0^{295}=4.049\,60$ Å using the data of Gibbons.[45]

IV. EXPERIMENTAL PROCEDURE

The experimental measurements were carried out in an ultrahigh-vacuum system constructed by Vacuum Generators with a 12-in.-diam μ-metal experimental chamber. The system included Varian four-grid LEED optics which were used for both LEED and retarding-field Auger-electron spectroscopy (AES) measurements.

The Al(210) crystal was mounted on a Vacuum Generators HPT2 manipulator with an x-y-z translation stage, with facilities for rotation about two orthogonal axes through the nominal crystal position, and with a tilt motion of the manipulator shaft about an axis perpendicular to the shaft at the top of the manipulator. The relative orientation of the LEED optics and manipulator was such that, with the tilt angle set to zero, the remaining

two rotations determined separately the incidence and azimuthal angles of the incident electron beam with respect to the crystal.

The Al(210) crystal was spark cut from a single-crystal rod obtained from Goodfellow Ltd. The orientation of the surface plane, as measured using an x-ray diffractometer, was refined to within 0.2° of the nominal orientation by mechanical and electrolytic polishing. The crystal, of dimension $7\times5\times1$ mm, was clamped under slight tension within a rectangular frame constructed by spot welding four 0.5-mm-diam W–25% Re pins. A W–5% Re/W–26% Re thermocouple was attached to the rear of the crystal by spot welding the 0.13-mm-diam thermocouple wires to a small piece of Al foil of thickness 0.05 mm, which was then spot welded to the crystal. The crystal support frame was mounted on the sample manipulator, which had facilities for heating the crystal by electron bombardment from the rear, and for cooling using liquid nitrogen.

After installation in the vacuum system, the crystal was cleaned by repeated cycles of Ar^+ sputtering (8×10^{-5} Torr Ar, 3-keV beam energy, 15-μA beam current) for 20 min, followed by annealing for 5 min at 800 K. After a total of 3 h sputtering, the only surface impurities detected in AES measurements (2-keV) beam energy, 50-μA beam current, 10-V peak-to-peak modulation) were small amounts of C and O. The peak-to-peak amplitudes of the C $KL_{23}L_{23}$ (270 eV) and O $KL_{23}L_{23}$ (510 eV) Auger lines were $<10^{-3}$ and $<5\times10^{-4}$, respectively, relative to the amplitude of the Al $L_{23}VV$ (68 eV) line.

When left to stand overnight in a vacuum of 1×10^{-10} Torr after cleaning, carbon and oxygen contamination levels were found to increase by about a factor of 2, although deliberate exposure to CO or CO_2 up to 10^{-4} Torr sec produced no measurable increase in the C and O AES signals. A single sputter-anneal cycle was sufficient to remove the contamination accumulated overnight before LEED measurements were performed. After completion of the cleaning procedure, the Al(210) crystal gave a sharp (1×1) LEED pattern.

LEED intensity-energy spectra were recorded by means of spot-photometric measurements of the light intensity produced by the diffracted beams at the fluorescent screen of the LEED optics. The spot photometer had an acceptance angle of 0.5°, and was positioned to give a measuring circle on the screen of about 3 mm diam as compared to the spot size of the diffracted beams of about 1 mm. In tracking a diffracted beam when changing the energy of the incident beam, the line of sight of the spot photometer to the beam spot was continuously adjusted to give a maximum signal in order to minimize the error due to the dependence of the light transmission through the grid system on the line of sight.

The diffraction geometry was set at normal incidence by means of comparative measurements of intensity-energy spectra for the 00 beam for a range of nominal values $\pm\theta$ of the angle of incidence, and by means of comparative measurements of intensity spectra for pairs of beams nominally related by the mirror-plane symmetry of the surface. To within the experimental reproducibility of the intensity spectra of about ±1 eV in peak positions and $\pm5\%$ in relative peak intensities, the diffracted beam intensities exhibited the full space-group symmetry of an ideal fcc (210) surface.

After establishing the condition of normal incidence, intensity-energy spectra were measured for 14 symmetry-inequivalent diffracted beams in the energy range 40–340 eV, with the crystal cooled to 135 K. The spectra were normalized for variations in the incident beam current and corrected for the measured background intensity. Plots of the experimental spectra are shown later in Fig. 4 together with plots of spectra calculated for the determined surface structure.

V. LEED INTENSITY CALCULATIONS

A. Computational model, input, and variables

Intensity-energy spectra were calculated using the layer-doubling method[46–48] in the energy range 30–350 eV (energies are given with respect to the vacuum level for a nominal inner potential of 10 eV) in steps of 0.3 Ry. The calculation of layer-scattering matrices, taking account of all intralayer multiple-scattering processes, was carried out using 12 phase shifts derived from the muffin-tin potential for Al of Moruzzi, Janak, and Williams.[49] The number of symmetry-inequivalent beams used in the calculation of interlayer multiple scattering, taking advantage of the mirror-plane symmetry,[47] was increased with energy from 43 at 30 eV to 80 at 206 eV, after which the number of beams was held fixed at 80 because of the length of the calculations. The corresponding numbers of symmetry-inequivalent beams propagating in the vacuum are 9, 43, and 74 at energies of 30, 206, and 350 eV, respectively. The convergence of the calculations was established by comparison with similar calculations made using 14 phase shifts and up to 131 symmetry-inequivalent beams.

The complex electron self-energy $\Sigma=V_0+iV_{im}$ was taken to be independent of energy, and a single Debye temperature Θ_D was used. The surface potential barrier was taken to be a refracting but nonreflecting potential step of height V_0.

Intensity-energy spectra were calculated for a total of 451 different surface structures in 41 computational runs, where the surface structure is specified by the values of the first five interlayer spacings d_1 to d_5 and interlayer registries r_1 to r_5. Each computational run involved the calculation of intensity spectra for 11 values of a particular structural variable d_i or r_i. These spectra were compared with the experimental spectra to determine the best-fit values of the structural variables, using the procedures described in Sec. VI.

In a few preliminary calculations, intensity spectra were calculated for a range of values of d_1, V_{im}, and Θ_D, after which the latter two variables were held fixed at the determined local optimum values of $V_{im}=4.0$ eV and $\Theta_D=600$ K.

B. Computational algorithm: Reuse of intermediate results

Considerable savings in computational effort were realized by dividing the calculations into three main stages.[36,42]

In the first stage, reflection and transmission matrices R_1, T_1 and R_2, T_2 were calculated for the two symmetry-inequivalent layers of which the crystal is composed, for each of 79 energy values in the energy range of interest. The matrices were written to disk at each energy.

In the second stage, the bulk reflection matrix R^B was calculated by means of the layer-doubling algorithm using the layer matrices R_1, T_1 and R_2, T_2 as input. This step requires approximately $(59v-33)b^3/6$ multiplications at each energy, where b is the number of beams carried in the calculation at a particular energy, and where v is the number of layer-doubling steps necessary to achieve convergence of the elements of R^B. Typically, v lies between 4 and 6, corresponding to a bulk crystal thickness of between 16 and 64 layers. At each energy, the matrices R_1, T_1 and R_2, T_2 were read from disk and R^B was written to disk. The total disk storage requirement for R_1, T_1, R_2, T_2, and R^B at all energies was 15.6 Mbyte. These matrices were subsequently reused in all of the intensity calculations made for the 451 different surface structures which were considered. Reading the five $b \times b$ complex matrices from disk at each energy required less than 1 CPU sec.

In the third and final stage of the algorithm, intensity-energy spectra were calculated for m different values of a particular interlayer spacing d_i or interlayer registry r_i in each computational run. This stage can be regarded as the joining of an N-layer selvedge to the bulk of the crystal. As shown schematically in Fig. 2, reflection and transmission matrices R_j^{-+}, R_j^{+-} and T_j^{++}, T_j^{--} are calculated for the surface slab consisting of the first j layers (for $j>1$) by means of a layer-addition algorithm,[48] using the layer matrices R_1, T_1 and R_2, T_2 as input. This step requires approximately $59(j-1)b^3/6$ multiplications. Next, a modified-bulk (MB) reflection matrix R_1^{MB} is calculated for the system composed of the $1=N-j$ deepest layers of the selvedge and the bulk of the crystal, using the layer matrices R_1, T_1, R_2, T_2, and the bulk reflection matrix R^B as input. This step requires approximately $9(N-j)b^3/2$ multiplications. Finally, the surface slab is jointed to the modified bulk and the diffracted intensities are calculated. This step requires approximately $4b^3/3$ multiplications. The surface slab matrices R_j^{-+}, R_j^{+-}, T_j^{++}, and T_j^{--}, hereafter S_j, and the modified-bulk reflection matrix R_1^{MB} are stored internally at each energy and reused in the intensity calculations for each of m values of d_j or r_j in a given computational run. Thus the total number of multiplications for the three steps of the final stage of the algorithm is $s_j \cong (26N+33j-59+8m)b^3/6$. It follows also that a set of $2N$ such computational runs in which intensity-energy spectra are calculated for m values of each of N interlayer spacings d_j and interlayer registries r_j requires

$$S \cong 2\sum_{j=1}^{N} s_j \cong 43N(N-1+8m)b^3/3$$

multiplications at each energy.

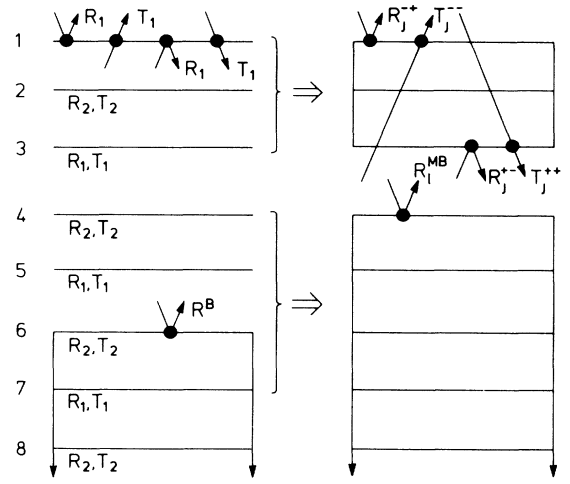

FIG. 2. Schematic of the calculation of intermediate scattering matrices in the calculation of intensity-energy spectra as a function of the interlayer spacing d_j or interlayer registry r_j for an N-layer selvedge. Here, $N=5$, $j=3$, and $l=2$. See text.

The above algorithm was implemented on a Norsk Data ND530/CX, 32-bit minicomputer with 1.25 Mbyte internal memory, and with a Whetstone benchmark performance of 0.6 MIPS (million instructions per second) according to the manufacturer. As noted previously, intensity-energy spectra were calculated for a total of 451 surface structures in 41 computational runs. The times for each run ranged from 12.8 CPU hours for $m=11$ values of d_1 or r_1 ($j=1, N=1$) to 42.4 CPU hours for 11 values of d_5 or r_5 ($j=5$, $N=5$). The observed CPU times scaled with the multiplication counts given above to within a maximum deviation of 8% from the mean. The total cost of the structure determination was 50 CPU days, including 6 and 35 CPU hours, respectively, for the initial calculations of the layer scattering matrices and the bulk reflection matrices in the first and second stages of the algorithm. In conventional LEED algorithms,[46,47] layer and bulk scattering matrices are stored internally at each energy and are also reused in calculating intensities for a range of values of a given structural variable. However, the matrices are overwritten at each subsequent energy. We estimate that the cost of the present structure determination with such an algorithm would be 120 CPU days. The corresponding cost using an algorithm without any reuse of intermediate results would be 820 CPU days (2.25 CPU years).

Although the present algorithm is considerably faster than conventional algorithms (by a factor of 2.4 for the present surface structure), it falls considerably short of what we believe could be achieved by a more systematic integration of the intensity calculations with the process of parameter optimization by comparison with experiment. Two obvious directions for improvement are discussed below in the context of the surface structure of interest here.

The first possibility would be to remove the limitation that the present scheme shares with conventional algorithms, namely that a set of values of a particular

structural variable must be specified before each computational run. A more efficient procedure, given a starting value for the variable in question, would be to put the choice of subsequent values in the control of a routine to optimize the fit between experiment and theory. The convergence to the local optimum value of the given variable would obviously depend upon the chosen starting value, but it seems likely that convergence would generally be reached in less than the 11 iterations used in the present work. An efficient implementation of such a scheme for the present surface structure would require extra storage of the surface slab matrices S_j and the modified-bulk reflection matrix R_1^{MB} at all energies. This would double the total disk storage from 15.6 to 31.2 Mbyte.

A second possibility for improvement would be to exploit the order in which the variables are considered, by making a further re-use of the results of intermediate calculations. For the present system, for example, an immediate reduction of computing time by a factor of 2 could be achieved by performing calculations for r_j after calculations for d_j if the appropriate matrices S_j and R_1^{MB} were saved at all energies. As noted above, this would require a total disk storage of 31.2 Mbyte. Further savings could be achieved by ordering the variables in the sequence $d_1, r_1, d_2, r_2, \ldots, d_N, r_N$. Thus, for example, prior to beginning a pass through the variables, the matrices R_1^{MB} for $1=1$ to $N-1$ could be sequentially calculated for all energies and stored on disk. This would require $\approx 9(N-1)b^3/2$ multiplications. Subsequently, for each value of $j>1$ the surface slab matrices S_j could be calculated for all energies and written to disk, using the previously calculated matrices S_{j-1} and the local optimum values of d_{j-1} and r_{j-1}. Each such step would require $59b^3/6$ multiplications for a total of $59(N-1)b^3/6$ multiplications for the complete pass. Thus the total number of multiplications required in the calculation of the S_j and R_1^{MB} would be $43(N-1)b^3/6$ at each energy as compared to the total of $43N(N-1)b^3/6$ required when S_j and R_1^{MB} are not available at all energies, giving a saving by a factor of N for this part of the calculation. For the present structure, assuming that $m=11$ values of d_j or r_j were considered in each run, the total saving would be a factor of 3.6 with respect to the current algorithm, and the total disk storage requirement would be 37.4 Mbyte.

Finally, we note our opinion that the systematic re-use of the intermediate results of LEED calculations can have as important an effect in reducing the cost of surface-structure determination as did the introduction of the exploitation of special conditions of symmetry.[50,51] In contrast to the latter, the programming changes that are necessary are straightforward, consisting largely of the introduction of symmetrical READ and WRITE statements, together with the division of a single main program into several main programs to be run in sequence.

VI. *R*-FACTOR PROCEDURES

The discrepancy between experimental and calculated intensity-energy spectra is measured using the statistic $\hat{R}_2$, defined below,[52] which is similar to one of the r factors used in x-ray crystallography,[53] and which we have found to be both numerically convenient and robust. The surface structure of Al(210) is determined by minimizing $\hat{R}_2$ as a function of the variables of the intensity calculations.

In assessing the suitability of $\hat{R}_2$ or any similar statistic the question arises of possible bias in the determination of the optimum values of the variables. We have established in the present work, as in previous studies, that our procedures using $\hat{R}_2$ lead to highly accurate (± 0.001 Å) retrieval of the input values of structural parameters when applied to comparisons of calculated spectra with *calculated* spectra. Comparative studies[35,54] of the use of $\hat{R}_2$ and alternative r factors in the analysis of experimental spectra have led to agreement in the structural conclusions to within estimated uncertainties. Such studies indicate also that $\hat{R}_2$ is not significantly less sensitive to the values of structural variables than r factors specially designed[55,56] for LEED. A brief comparison of the results obtained using $\hat{R}_2$ with those obtained using the r factor suggested by Pendry[56] is presented in Sec. VIII.

In the remainder of this section, after definition of $\hat{R}_2$, the procedures for determination of the optimum values of the variables and their standard deviations are described and discussed. In particular, it is argued that a potential advantage of $\hat{R}_2$ is its use in conjunction with the method of least squares to provide estimates of standard deviations, which do not depend on assumptions concerning the nature of the intensity spectra or the diffraction process. Although it has not been possible to fully implement the advocated procedure in the present work, we believe that its discussion here might be useful in influencing future studies.

A. Definition of the *r* factor

The discrepancy between experimental $I^{\mathrm{expt}}(E)$ and calculated $I^{\mathrm{calc}}(E)$ intensity-energy spectra for a particular hk beam is measured by

$$R_2 = \sum_i [w_i(I_i^{\mathrm{expt}} - c_{hk} I_i^{\mathrm{calc}})]^2 , \tag{6.1}$$

where c_{hk} is a scaling factor given by

$$c_{hk} = \sum_i I_i^{\mathrm{expt}} \Big/ \sum_i I_i^{\mathrm{calc}} . \tag{6.2}$$

The inverse of the weights w_i in Eq. (6.1) should properly be equal to or proportional to the standard deviations σ_i of the data points. Although we see no difficulty in principle in making an empirical determination of the σ_i by simply repeating the measurements a sufficient number of times, this was not practical with our relatively crude measuring technique, nor have such measurements been made in other LEED studies to the best of our knowledge. We hope to examine this question in future studies using a video-LEED system now under construction.

In the absence of measurements of the σ_i, the weights w_i in Eq. (6.1) are taken to be

$$w_i = 1 \Big/ \sum_i (I_i^{\mathrm{expt}})^2 , \tag{6.3}$$

implying equal standard deviations of the data points for a given beam. For convenience, the summations of Eqs. (6.1)–(6.3) were carried out after interpolation of the spectra on to a common energy grid for N_{hk} data points with interval 0.5 eV.

The quantity that is minimized in the determination of the optimum values of the variables is the beam-average r factor defined by

$$\hat{R}_2 \equiv R = (1/N) \sum_{h,k} N_{hk} R_2 \ , \tag{6.4}$$

where

$$N = \sum_{h,k} N_{hk} \ . \tag{6.5}$$

B. Determination of the optimum parameter values

Following the method of least squares, the optimum parameter values x_n^0 are found by requiring that $g_n = 0$ for all n, where

$$g_n = \partial R / \partial x_n \ . \tag{6.6}$$

Determination of the x_n^0 is facilitated by assuming R to be a quadratic function of the variables in the neighborhood of the global minimum at $\underline{x}^0$ with value R^0. Thus

$$R(\underline{x}) = R^0 + \tfrac{1}{2}(\underline{x} - \underline{x}^0)^T \underline{G} (\underline{x} - \underline{x}^0) \ , \tag{6.7}$$

where the curvature matrix $\underline{G}$ has the elements

$$G_{nm} = \partial^2 R / \partial x_n \partial x_m \ . \tag{6.8}$$

The optimum parameter values are then given by

$$\underline{x} - \underline{x}^0 = \underline{\varepsilon}[\underline{x}^0] \underline{g}[\underline{x}] \ , \tag{6.9}$$

where the error matrix $\underline{\varepsilon}$ is given by

$$\underline{\varepsilon} = \underline{G}^{-1} \ . \tag{6.10}$$

As in previous studies,[10] computed values of $R(\underline{x})$ are found here to be described to an excellent approximation by Eq. (6.7). The uncertainty in the optimum values of the variables resulting from the deviation of $R(\underline{x})$ from quadratic behavior is typically of order 0.001 Å and can be neglected.

Although the optimum parameter values can in principle be obtained in a single step via Eq. (6.9), given $\underline{G}[\underline{x}]$ and $\underline{g}[\underline{x}]$ for arbitrary $\underline{x}$, in practice it cannot be assumed that $\underline{G}[\underline{x}] = \underline{G}[\underline{x}^0]$, since $\underline{x}$ may lie outside the region of quadratic behavior. Thus standard algorithms for nonlinear minimization based on Eq. (6.9) generally involve implicit or explicit construction of $\underline{G}[\underline{x}^0]$ by an iterative process.

The expense of accurate calculations of LEED intensities has so far precluded the use of minimization methods based on Eq. (6.9), which requires evaluation of all the elements of the curvature matrix $\underline{G}$, except for a single application in the determination of the surface structure of Al(110).[10] Thus, as in a number of previous studies,[42] a simple grid-search procedure based on Eq. (6.7) is used here. In each step of the procedure the local optimum value of a *single* structure variable, d_i or r_i, together with the corresponding local optimum value of the inner potential V_0 is determined by fitting[52] an elliptic paraboloid to the variation of R with d_i or r_i and V_0, with the remaining variables held fixed at their previously determined local optimum values. The procedure is carried out for each variable in turn and iterated to convergence.

It is evident that the rate of convergence of such an algorithm depends both upon the size of the correlations between the variables, and upon the relative sensitivity of the r factor to the different variables. It is also evident that there is a risk of straying into a region of parameter space containing a spurious local minimum. The risk is presumably reduced by carrying out the optimization of the variables in the order of decreasing sensitivity of the r factor to the variables. In the present case, as described later, the sensitivity to d_i and r_i decreases generally, although not completely uniformly, with increasing layer index i as might be expected. For more complicated structures, the ordering of the variables with respect to their relative sensitivity may be much less obvious. We note, however, that the relative sensitivity of the r factor to a particular variable depends largely on the gradients of the calculated intensities with respect to the variables, which may allow reasonable estimates of the relative sensitivities to be made from the calculated intensities alone.

C. Determination of the estimated standard deviations

Comparison with the results of other experimental methods (see table I, for example) suggests that the accuracy of surface structure determination by LEED in the case of simple structures may be of the order of a few hundreds of an angstrom. This notwithstanding, the analysis of the internal precision of the results is in our opinion one of the least satisfactory aspects of current methodology. Estimates of precision are generally based on either more or less educated guesses, or on various *ad hoc* assumptions regarding the information content of LEED intensity-energy spectra. In addition, the contribution of correlations between the variables to the uncertainty of their optimum values is either ignored or treated incompletely.

This situation is due in part to the expense of calculations of LEED intensities. Thus treatment of the correlations between the variables requires evaluation of all the elements of the curvature matrix $\underline{G}$ in Eq. (6.8). This in turn requires many more intensity calculations than are normally carried out in current structure determinations. For the relatively simple surface structure of Al(110), where a detailed study of correlations was made,[10] it was found that 30–40 % of the estimated standard deviations of the structural variables could be attributed to correlations. For more complicated structures it seems likely that ignoring correlations might well lead to underestimation of standard deviations by a factor of two or more. In the present work, because of the expense of the intensity calculations, only the correlations between a particular interlayer spacing d_i or registry r_i and the inner potential V_0 were taken into account.

The more fundamental problem, however, appears to be the lack of a generally accepted framework for treat-

ing the question of precision. This in our opinion is a consequence of the wide-spread use of unnecessarily complicated r factors.[55,56] We believe that use of the simple $\hat{R}_2$ statistic in conjunction with the method of least squares, as discussed below, provides in principle a straightforward means for obtaining objective estimates of the standard deviations of optimum parameter values. We confess, however, that our hopefully improved understanding of the method postdates the present experimental measurements, with result that certain necessary conditions are not fulfilled by the measurements and that therefore the standard deviations are determined here only to within an unknown scale factor.

According to the method of least squares, the standard deviations σ_{x_n} of the optimum values x_n^0 of the variables depend on the diagonal elements ε_{nn} of the error matrix $\underline{\varepsilon}$ via

$$\sigma_{x_n}^2 = \varepsilon_{nn} R^0 / N_F \ , \tag{6.11}$$

where the number of degrees of freedom N_F is given by

$$N_F = N_D - \nu \ , \tag{6.12}$$

where ν is the number of variables, and where N_D is the number of independent observations.

Estimation of σ_{x_n} by Eq. (6.11) requires then a definition of the number of "independent observations" N_D. Most discussions of this question, including some previous work from this laboratory, have been based on the premise that N_D is related to the number of peaks in the intensity-energy spectra, rather than simply equal to the number of intensity-energy data points (assuming a discrete energy grid). Since intensity-energy spectra usually contain overlapping peaks, definition of N_D then involves the question of how the number of peaks should be counted.

The reason for identifying N_D with the number of peaks rather than with the number of data points appears to be the notion that since the intensities at adjacent energy values are correlated, they do not constitute independent measurements. Such correlations, however, exist between the intensities at *all* energies and in all beams. They follow simply from the nature of the diffraction process, and are irrelevant in the context of a discussion of the precision of structure determination. What is relevant in this context is the extent of correlations between the *uncertainties* in the measured intensities at adjacent energies as introduced by the instrumental response, in particular by the energy spread of the incident electron beam.

Thus we believe that there is no fundamental obstacle to a proper definition of N_D in Eq. (6.12). On condition that the summation of Eq. (6.1) is carried out on the same discrete energy grid as the experimental measurements, without any smoothing of the data, and on condition that the energy interval is large enough (say 0.5 to 1.0 eV) to avoid the introduction of correlations between the uncertainties of adjacent intensities by the instrumental response, then N_D is simply equal to the number of data points N in Eq. (6.5).

In the present work the above conditions were not satisfied, because of the quasicontinuous nature of the measurements and because of the smoothing resulting from interpolation of the intensities. Thus, as in previous structure determinations made in this laboratory,[42] N_D is taken here to be equal to the number of kinematic Bragg peaks contained within the energy range of the measurements, as calculated for an ideal, truncated-bulk crystal. This leads undoubtedly to an underestimate of N_D and hence to an overestimate of σ_{x_n}, which probably more than compensates for the incomplete treatment of correlations between the variables.

Finally, it is convenient to define a dimensionless measure of the sensitivity of $\hat{R}_2$ to a given variable x_n by

$$s_n = x_n^0 / \sigma_{x_n} \ , \tag{6.13}$$

where for $g_{m \neq n} = 0$ it follows that

$$s_n = [N_F (R(\underline{x}) - R^0)]^{1/2} / [(x_n - x_n^0)/x_n^0] \ . \tag{6.14}$$

VII. ANALYSES OF THE EXPERIMENTAL DATA

A. *R*-factor minimization

The surface structure of Al (210) was determined by minimizing $\hat{R}_2$ as a function of the first five interlayer spacings d_n and registries r_n and inner potential V_0 by means of the iterative procedure described in Sec. VI.

The course of the optimization of d_1 to d_5 and r_1 to r_5 is summarized in Table IV. Apart from the entries for iteration 0 in the first row, which contain the bulk values d_B and r_B, each entry is the result of an elementary iteration step in which the r-factor was minimized with respect to a single structural variable d_n or r_n together with V_0. For compactness, the results are grouped in rows as iterations 1–5, each containing the results of several elementary steps, the sequence being from left to

TABLE IV. Iterative refinement of the surface structure of Al(210).

Iteration	d_1 (Å)	r_1 (Å)	d_2 (Å)	r_2 (Å)	d_3 (Å)	r_3 (Å)	d_4 (Å)	r_4 (Å)	d_5 (Å)	r_5 (Å)	V_0 (eV)	$\hat{R}_2$
0	0.903	1.805	0.903	1.805	0.903	1.805	0.903	1.805	0.903	1.805	4.5	0.4470
1	0.752	1.727	0.926	1.745	0.957	1.847	0.878	1.790			7.4	0.1346
2	0.755		0.908		0.974		0.866				7.7	0.1217
3	0.758	1.787	0.904	1.736	0.981	1.835	0.863	1.780			7.6	0.1074
4	0.761	1.802	0.898	1.740	0.983	1.832	0.862	1.772	0.894	1.796	7.8	0.1056
5	0.762	1.804	0.895	1.748	0.983	1.835	0.863	1.769	0.892	1.789	7.9	0.1052

right along the rows. The running optimum values of V_0 and $\hat{R}_2$ are listed only at the end of each of the five master iterations.

The ranges of parameter variation in each of the iteration steps are given in Table V. Eleven or more values of a structural variable were considered in each step, with grid spacing decreasing from 0.01 to 0.04 Å in iteration 1 to 0.005 Å to iteration 5.

Inspection of the results for the individual variables in the columns of Table IV indicates a fairly uniform passage to convergence, except for r_1 and d_2 for which rather large changes occurred after the first iteration. After completion of the work summarized in the table, a final variation of d_1 was carried out, using intensities calculated with 14 phase shifts and up to 131 symmetry-inequivalent beams, giving optimum values of $d_1=0.763$ Å, $V_0=7.9$ eV, and $\hat{R}=0.1041$.

The dependence of $\hat{R}_2$ on the interlayer spacings and registries, as calculated in the final iteration of Table IV, is plotted in Figs. 3(a) and 3(b), respectively. Plots of the experimental intensity-energy spectra and spectra calculated for the optimum surface structure are shown in Fig. 4. As can be seen from the plots, the experimental spectra are rich in structure, most of which is reproduced in the calculated spectra, although rather large discrepancies in the relative intensities occur for some of the beams.

B. Optimum parameter values

The optimum parameter values and estimated standard deviations obtained by minimization of $\hat{R}_2$ are listed in Table VI. As a check on these results, the intensity calculations made in the final iteration of Table IV were reused to determine optimum parameter values by minimization of the r factor of Pendry[56] R_p, with results also listed in Table VI. As can be seen, the optimum values obtained using the two different r factors are in reasonable agreement. It should be emphasized, however, that a proper comparison with $\hat{R}_2$ would require a full, independent minimization of R_p, which was not carried out.

Also listed in Table VI are the sensitivities s_n of $\hat{R}_2$ and R_p to the different variables, as calculated using Eq. (6.14) and normalized by setting $s_{d_1}(\hat{R}_2)=100$ to remove the dependence on N_F. It can be seen that an overall decrease in sensitivity with layer index occurs for each r factor, except for the anomalously large sensitivities to d_3 and r_3. It is noted that the average sensitivity of R_p to the structural variables is about 5% greater than that of $\hat{R}_2$.

The displacements of surface atoms from their bulk positions, as calculated from the interlayer spacings and registries given in Table VI, are shown schematically in Fig. 5.

C. Estimated standard deviations

The standard deviations of the optimum parameter values listed in Table VI were estimated using Eqs. (6.11) and (6.12) with $N_D=24$, $v=11$ and hence $N_F=13$. As discussed in Sec. VI, these estimates are probably very conservative because of the underestimate of N_D made here.

As a check on the values given in Table VI, the intensity calculations made in the final iteration of Table IV were used to determine optimum parameter values by separate minimization of the r factors for the individual diffracted beams. The mean values of the results, and the standard deviations obtained from the dispersions about the mean values, are listed in Table VII together with the results, given previously in Table VI, obtained by minimization of the beam-average r factor.

In comparing the values given in the tables, it must be emphasized that the results obtained for the individual beams are of limited significance, in that they cannot be regarded as truly independent measurements since they were not obtained by fully independent minimizations of R_2. Such independent minimizations are unfortunately impractical, partly because they would require a factor of about b more intensity calculations, where $b=14$ is the number of diffracted beams in the present data set, and partly because the dependence of R_2 on the variables is generally much less well behaved than that of $\hat{R}_2$, probably due to an increase in the correlations between the variables associated with the smaller amounts of data being analyzed. The latter difficulty is illustrated by the fact that only in the cases of d_1 and d_3 were well-defined minima of R_2 obtained for all the diffracted beams. The number of beams n_b for which well-defined minima were

TABLE V. Ranges and increments (Å) of parameter variation, for iterations $i=1-5$.

x_n	$i=1$	$i=2$	$i=3$	$i=4$	$i=5$
d_1	0.70–0.90,0.02	0.74–0.82,0.01	0.74–0.79,0.005	0.74–0.79,0.005	0.74–0.79,0.005
r_1	1.65–1.86,0.02		1.68–1.81,0.01	1.74–1.84,0.01	1.78–1.83,0.005
d_2	0.80–1.00,0.02	0.85–0.95,0.01	0.85–0.95,0.01	0.875–0.925,0.005	0.87–0.92,0.005
r_2	1.55–1.95,0.04		1.71–1.81,0.01	1.705–1.755,0.005	1.715–1.765,0.005
d_3	0.85–1.05,0.02	0.91–1.01,0.01	0.93–1.03,0.01	0.96–1.01,0.005	0.96–1.01,0.005
r_3	1.70–1.90,0.02		1.79–1.89,0.01	1.805–1.855,0.005	1.81–1.86,0.005
d_4	0.81–0.91,0.01	0.82–0.92,0.01	0.83–0.89,0.005	0.835–0.885,0.005	0.835–0.885,0.005
r_4	1.72–1.92,0.02		1.74–1.84,0.01	1.75–1.80,0.005	1.745–1.795,0.005
d_5				0.82–0.92,0.01	0.865–0.915,0.005
r_5				1.75–1.85,0.01	1.77–1.82,0.005

found for the different variables is listed in Table VII,

The above-mentioned qualifications notwithstanding, we consider that the relatively small dispersion of the results for the individual beams is certainly consistent with the conclusion made above, that the standard deviations estimated using the beam-average r factor $\hat{R}_2$ are conservative.

VIII. DISCUSSION

A. Comparison of the present results with theoretical predictions for the surface structure of Al(210)

As noted previously, a major purpose of the present work was to test the prediction for the surface structure of Al(210) made by Barnett *et al.*[1] After our work was completed, we were kindly informed by Franco Jona of the results of calculations of surface structure for a number of Fe and Al surfaces, including Al(210), carried out by Jiang, Marcus, and Jona,[57,58] to which comparison is also made below.

The model used by Jiang *et al.* is a modification of the simplest model considered by Landman *et al.*,[14] involving calculation of the electrostatic interactions between nets of point ions and a uniform, frozen, electron charge density which terminates in a step at the surface. It does not include the pseudopotential corrections incorporated in the calculations of Barnett *et al.*[1] for Al(210). The modification consists of the inclusion of an empirical factor α which weights the relative contribution to the surface energy resulting from displacement of nets of ions from their bulk equilibrium positions at the center of slabs of neutralizing electron charge density of thickness equal to the bulk interlayer spacing. Values of α greater than unity reduce the relaxations that would otherwise be predicted by the unmodified point-ion model. Jiang *et al.* find that a value of $\alpha=1.9$ leads to remarkable agreement with most of the relaxations measured for the six most close-packed surfaces of both Fe and Al.

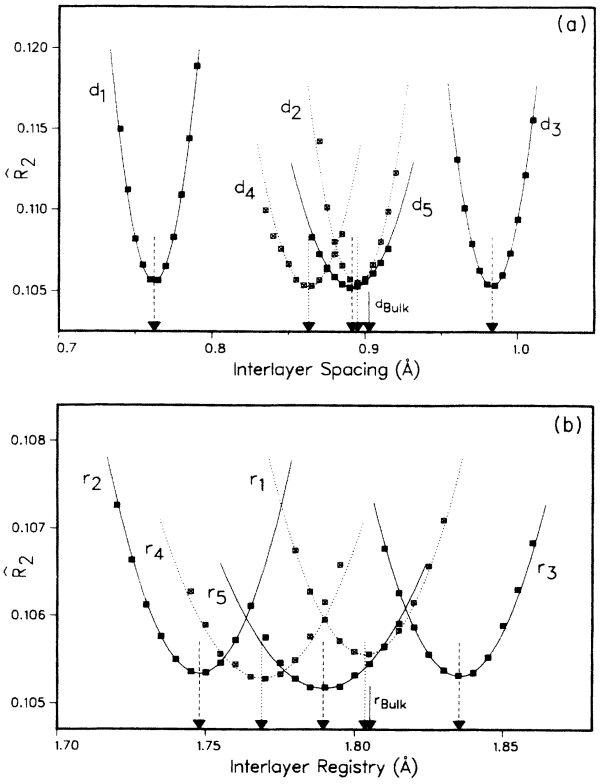

FIG. 3. (a) Plots of $\hat{R}_2(\partial\hat{R}_2/\partial V_0=0)$ vs the interlayer spacings d_1-d_5 and (b) vs the interlayer registries r_1-r_5, constructed from the results of the final iteration of Table IV. The dashed lines indicate the optimum values of d_1-d_5 and r_1-r_5. The corresponding bulk values are indicated by solid lines. The plotted curves are least-squares parabolas fitted to the computed $\hat{R}_2$ values (squares).

The relaxations determined in the present work are listed together with the predictions of Barnett *et al.*[1] and Jiang *et al.*[57] in Table VIII, and are plotted in Fig. 6. As can be seen from these comparisons, the trends of the experimental results are reproduced by both sets of calculations. The experimental relaxations are generally smaller than those predicted by Barnett *et al.*, but near-quantitative agreement exists with the calculations of Jiang *et al.*

Also listed in Table VIII are calculations[59] of the forces on the surface layers of the *unrelaxed* structure made using the point-ion model, as discussed in Sec. VIII C, which also lead to a correct prediction of the trends of the relaxations.

In addition to the theoretical studies noted above, calculations of the surface structure of a number of Al surfaces have been reported recently by Chen, Voter, and Srolovitz[60] using the embedded-atom method of Daw and Baskes.[61] No tabulation of the results for Al(210) is given in the article by Chen *et al.*, but inspection of their Fig. 1 indicates that the trends in the calculated relaxations of the interlayer spacings, if not the magnitudes, are in agreement with the present experimental results.

B. Trends in the multilayer relaxations of Al and Fe surfaces

With the completion of the present work, experimental determinations of surface structure are now available for the six most close-packed surfaces of Al. The possibility of multilayer relaxation has been examined for four of these surfaces, the exceptions being the most close-packed (111) and (100) surfaces[5,62,63] which appear to correspond to almost perfect truncations of the bulk crystal structure.

The trends in the relaxation of the four more open Al(110),[10,18] (311),[37] (331),[42] and (210) surfaces can be seen in Fig. 7, where the relaxations of the interlayer spacings are plotted as a function of depth. The oscillatory nature of the relaxations is evident from the figure. It can also be seen that the relaxations are damped to zero within 4–5 Å from the surface. Very similar conclusions apply to the relaxation of the interlayer spacings of the open surfaces of Fe, as can be seen from the plot of Fig. 8, constructed from the results of Jona and coworkers.[38,41]

A direct comparison of the relaxations of the interlayer spacings of the six most close-packed surfaces of Al and Fe is given in Table IX, where the number of missing

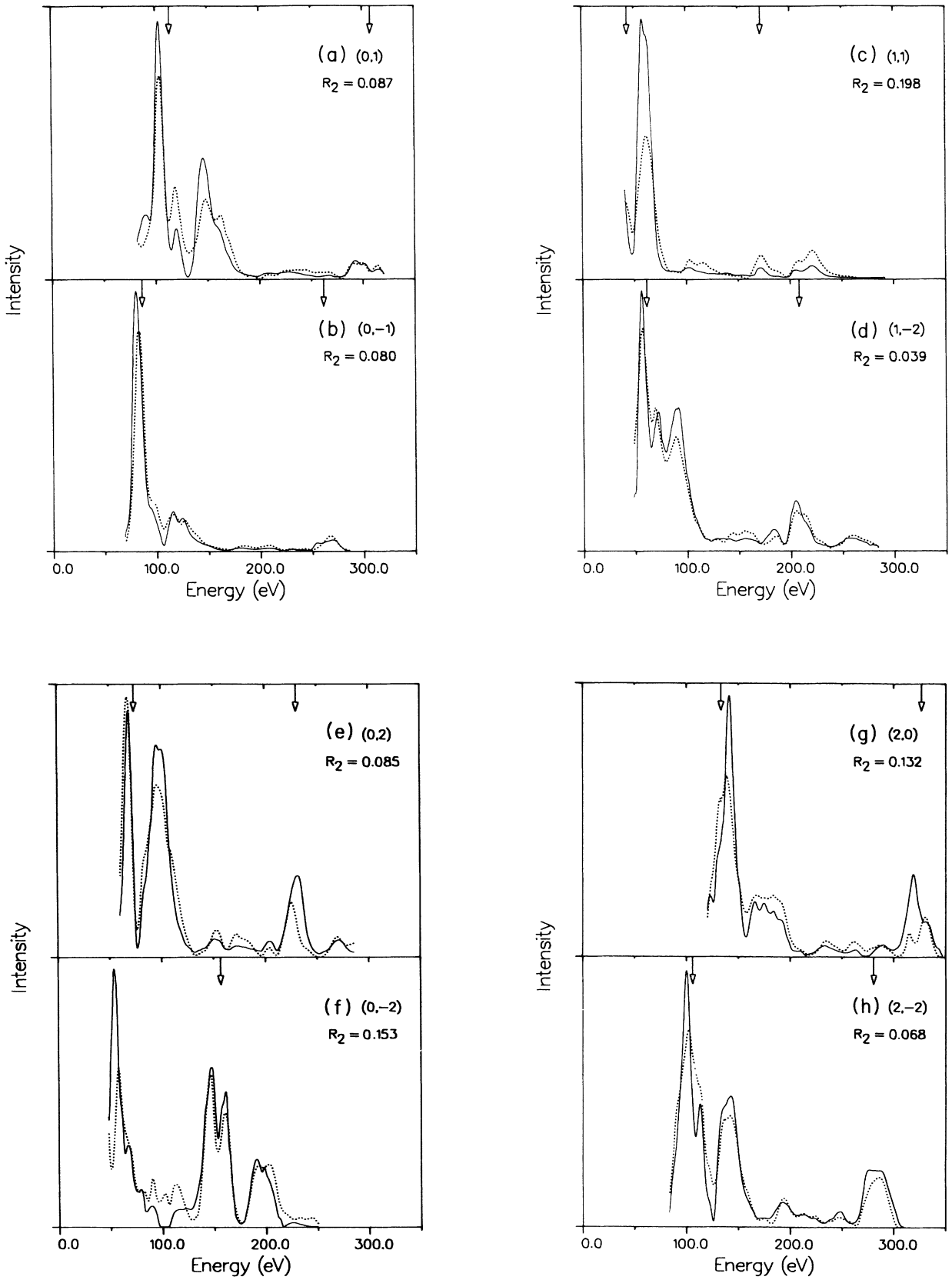

FIG. 4. (a)–(n) Comparison of experimental intensity-energy spectra (solid curves) with spectra (dotted curves) calculated for optimum values of the calculational variables (see Table VI). In each plot, the experimental and calculated spectra have been normalized to equal integrated area. Beam indices and computed R_2 values for the individual beams are given in the figures. Downward arrows indicate the positions of kinematics Bragg peaks calculated for a truncated-bulk structure.

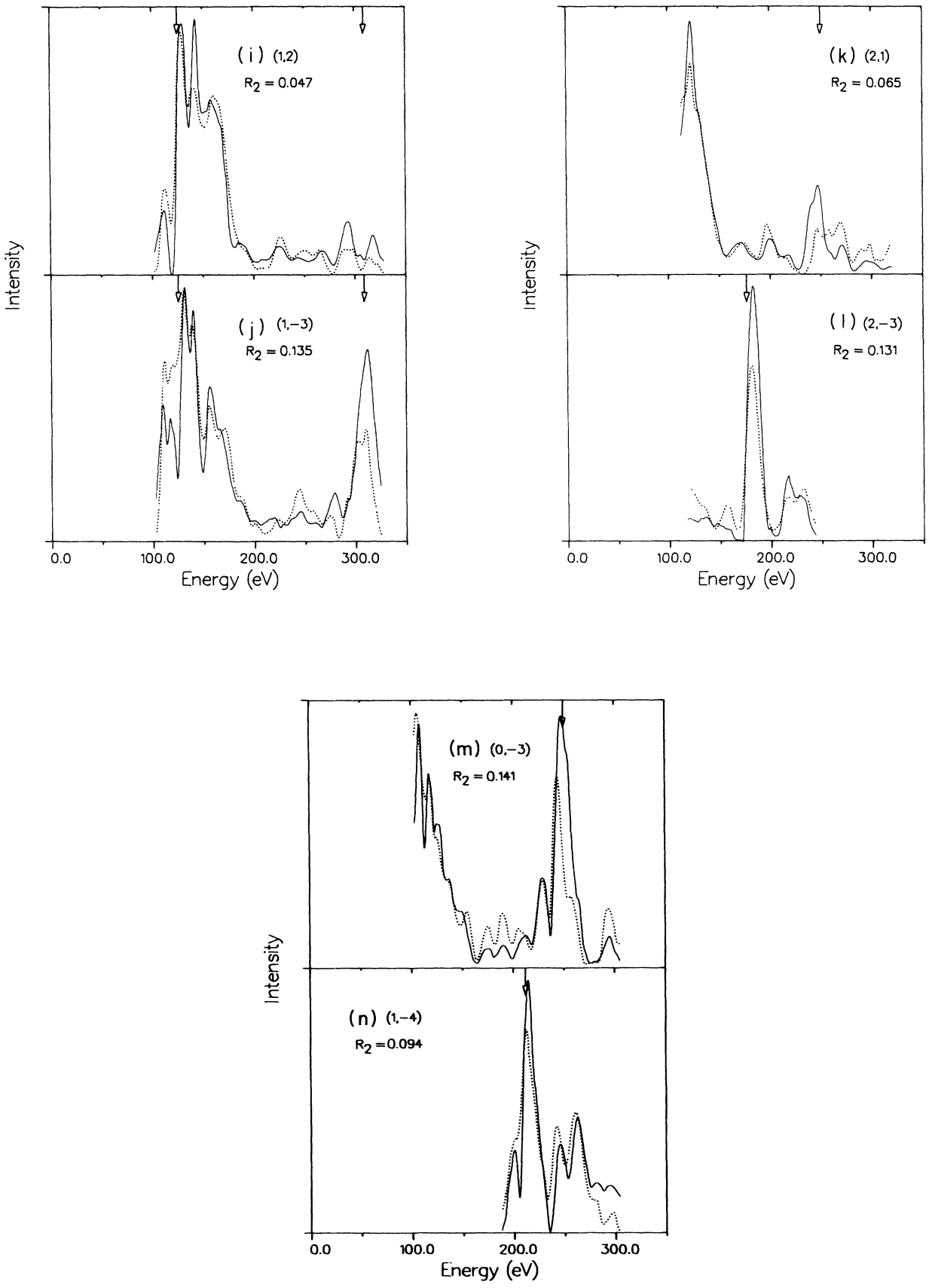

FIG. 4. (*Continued*).

TABLE VI. Optimum parameter values and sensitivities.

	$\hat{R}_2$			R_p	
x_n	x_n^0 (Å)	σ_{x_n} (Å)	s_n	x_n^0 (Å)	s_n
d_1	0.763	0.022	100	0.766	80
d_2	0.895	0.027	96	0.915	86
d_3	0.983	0.023	120	0.993	110
d_4	0.863	0.032	76	0.869	93
d_5	0.892	0.041	59	0.906	78
(d_B=0.903 Å)					
r_1	1.804	0.062	83	1.793	92
r_2	1.748	0.060	89	1.728	59
r_3	1.835	0.056	94	1.811	131
r_4	1.769	0.072	77	1.765	80
r_5	1.789	0.083	63	1.777	92
(r_B=1.805 Å)					
V_0	7.9 eV	1.0 eV			

nearest neighbors per atom in the surface layers is also listed for each surface. The similarity in the relaxation trends for Al and Fe, except for the (100) planes, is evident from this comparison. It can be seen that the depth of the relaxations appears to be correlated with the number of planes containing atoms with less than their full complement of nearest neighbors. Except for the close-packed Al(111) and (100) and Fe(110) surfaces, the relaxations generally extend to and include the first layer of atoms with a full complement of nearest neighbors. Since the atoms in such layers have nearest-neighbor atoms in the first layer, simple geometric considerations suggest that the inward movement of such "bulk" atoms might be a response to the inward movement of the atoms of the first layer (see Figs. 1 and 5). It can also be seen that the magnitude of the relaxations increases generally with the total number of missing nearest neighbors associated with the unit mesh. With respect to the relaxation sequence, it can be noted that this changes from $-+-$ for the surfaces having two planes containing atoms with missing nearest neighbors to $--+-$ for the more open surfaces having three such planes.

Finally, however, it must be noted that the similarity in the relaxation trends of Al and Fe surfaces does not extend to the relaxation of the interlayer registries. These are much larger for Fe than for Al, but there appear otherwise to be no obvious trends in the results.

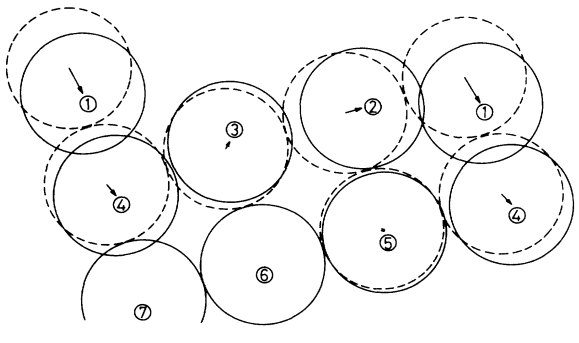

FIG. 5. Hard-sphere model of the determined surface structure as projected on the (001) mirror plane. Solid circles indicate the positions of atoms in the relaxed structure, and open circles indicate the corresponding positions in the ideal, unrelaxed structure. The direction of the atomic displacements, which are all contained within the (001) plane, are indicated by arrows. The displacements are exaggerated by 5 times in the figure.

C. Towards an intuitive description of multilayer relaxation

In this section we examine the possibility that the relaxation sequence for a given surface can be predicted from the properties of the ideal, *unrelaxed* structure by simply physical arguments. In view of the complexity of self-consistent, total-energy calculations of surface structure, this goal might appear to be naive. Nevertheless, the apparently weak material dependence of the relaxation trends, as indicated by the results described in Sec. VIII B and in Sec. II, encourages the belief that simple geometrical factors play an important role, as does the success of semiempirical models in rationalizing the experimental results. In the following we consider the physical insight provided by models of the effective-medium type, and also by simple electrostatic models.

The apparent correlation of the trends in the relaxation of interlayer spacings with the number of missing nearest-neighbors in the surface layers suggests models of the effective-medium[64] or embedded-atom[61] type as natural vehicles for obtaining physical insight. In the effective-medium theory[64] the atomic binding energy is given by the embedding energy of the atom in a homogeneous electron gas of the appropriate density, together with correction terms. The embedding energy is known as a function of density from the results of self-consistent calculations. In a solid, the density is taken to be that re-

TABLE VII. Comparison of optimum parameter values and standard deviations obtained by minimization of $\hat{R}_2$ with values obtained by minimization of R_2 for the individual diffracted beams.

x_n	$x_n^0(\hat{R}_2)$ (Å)	$x_n^0(\hat{R}_2)$ (Å)	n_b
d_1	0.763±0.022	0.766±0.005	14
d_2	0.895±0.027	0.903±0.007	13
d_3	0.983±0.023	0.985±0.007	14
d_4	0.863±0.032	0.871±0.008	12
d_5	0.892±0.041	0.907±0.008	12
r_1	1.804±0.062	1.824±0.016	8
r_2	1.748±0.060	1.743±0.016	9
r_3	1.835±0.056	1.825±0.013	8
r_4	1.769±0.072	1.769±0.017	8
r_5	1.789±0.083	1.791±0.017	9
V_0	7.9 ±1.0 eV	7.4 ±0.1 eV	

sulting from a superposition of densities setup by neighboring atoms.

In an application of the theory to the surface structures of Al(111), (100), and (110), Jacobsen, Nørskov, and Puska[64] explain their calculated relaxations in terms of a competition between the density-dependent embedding-energy term and an atomic-sphere correction term, both of which depend on the number and configuration of nearest neighbors. Thus the contraction of the first interlayer spacing of Al(110) is attributed to an inward movement of the atoms in the first layer toward a region of higher electron density, since the atoms of the first layer lack five nearest neighbors and therefore sample a less than optimal density. This inward movement is opposed by the atomic-sphere correction because the atomic spheres of first- and second-layer atoms begin to overlap. The correction term, together with the increased electron density resulting from the inward movement of the first layer is responsible for the outward movement of the second layer. Jacobsen *et al.* suggest further that similar arguments can be applied to rationalize the more complicated − − + relaxation sequences found for more open surfaces.

Without questioning the plausibility of these suggestions, we note that they invoke the self-consistent adjustment of the relative positions of surface layers, the result of which depends upon the balance between the embedding-energy and atomic-sphere terms. Thus definite prediction of the relaxation sequence for a given surface has not been made based on intuitive arguments alone, that is, without carrying out a self-consistent minimization of the surface energy as a function of the layer positions.

At present, the simplest description of multilayer relaxation is to be found in the point-ion–frozen-background model. As noted previously, Jiang *et al.*[58] have obtained remarkable agreement with experimental results for Al and Fe surfaces, using a simple modification of the mod-

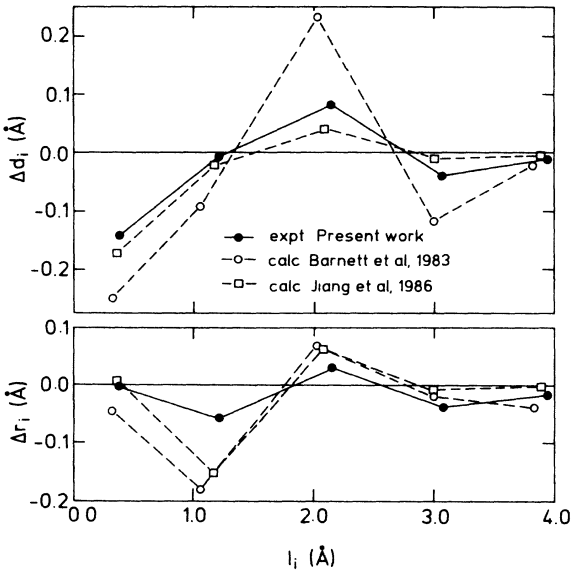

FIG. 6. Comparison of experimental (present work) and calculated relaxations Δd_i and Δr_i of the interlayer spacings and registries, plotted against the layer midpoint depths l_i.

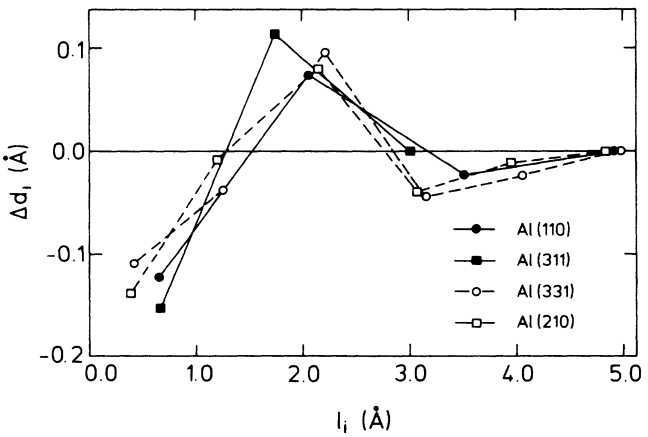

FIG. 7. Relaxations of the interlayer spacings of Al surfaces plotted against the layer midpoint depths.

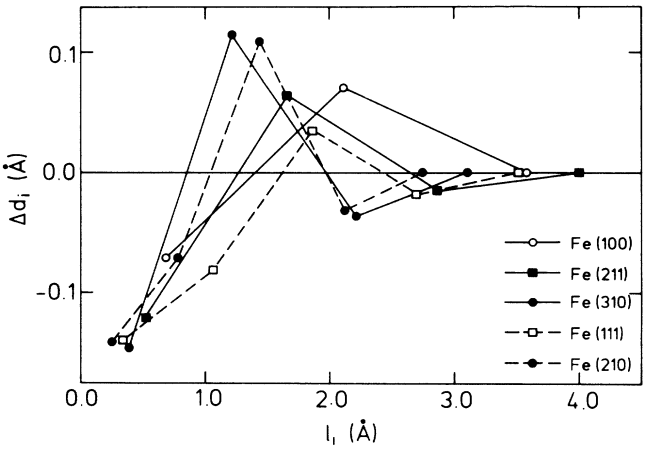

FIG. 8. Relaxations of the interlayer spacings of Fe surfaces plotted against the layer midpoint depths.

el. In fact, in response to remarks made previously[42] by one of the present authors, Jiang *et al.* conclude that "the desired insight and predictive power is achieved by our modified point-ion model." The present authors, however, taking a simple view, are frustrated by the fact that, given the simplicity of the model, it is still necessary to carry out a self-consistent minimization of the surface energy to predict, for example, the qualitative trends of the relaxation of Al(210). In the following, therefore, we examine the extent to which these trends can be deduced from the electrostatic forces on the layers of the *unrelaxed* surface.

We consider, therefore, the electrostatic forces between infinite, equivalent, Bravais nets of ions of charge Z, embedded in slabs of neutralizing charge of thickness d equal to the bulk interlayer spacing. The electrostatic potential in the plane of the mth net due to the charge in the nth layer is given by the Madelung equation[65] as

$$\Phi(\mathbf{r}_{nm})=\frac{4\pi Z}{A}\sum_{\mathbf{g}}{}''\, g^{-1}e^{-g\,|\,z_{mn}\,|}\cos(g_x x_{mn}+g_y y_{mn}), \tag{8.1}$$

where $\mathbf{r}_{mn}$ is a vector from an origin in the nth net to a point in the mth net, with components x_{mn},y_{mn},z_{mn} along orthogonal axes, where the xy plane is parallel to the surface and the z axis is along the outward surface-normal direction. In Eq. (8.1), A is the area of the primitive unit mesh. The summation is over the reciprocal-net vectors $\mathbf{g}$. The symbol $\sum''$ denotes the exclusion of $\mathbf{g}=\mathbf{0}$ and, for a given $\mathbf{g}$, the exclusion of $-\mathbf{g}$. The former condition follows from the charge neutrality of the layers, and the second from the inversion symmetry of the Bravais nets.

The electrostatic force $\mathbf{F}_{mn}$ on an ion in the mth net due to the potential of the nth layer is, therefore,

$$\mathbf{F}_{mn}=-Z\nabla\Phi(\mathbf{r}_{mn})\ . \tag{8.2}$$

Restricting attention to the forces on the ions in the *unrelaxed* structure, it follows simply that these have components

$$F^0_{mn}(z)=\mathrm{sgn}(n-m)\frac{4\pi Z^2}{A}\times\sum_{\mathbf{g}}{}''\, e^{-|\,m-n\,|gd}\cos[(m-n)\mathbf{g}\cdot\mathbf{v}] \tag{8.3}$$

and

$$F^0_{mn}(x)=\frac{4\pi z^2}{A}\sum_{\mathbf{g}}{}''\left[\frac{g_x}{g}\right]e^{-|\,m-n\,|gd}\sin[(m-n)\mathbf{g}\cdot\mathbf{v}]$$

with a similar equation for $F^0_{mn}(y)$ obtained by replacing x by y in the equation for $F^0_{mn}(x)$. In Eq. (8.3), $\mathbf{v}$ is the projection on the xy plane of the vector $\mathbf{s}$ connecting origins in successive nets. It follows simply from Eq. (8.3) that $\mathbf{F}^0_{mn}=-\mathbf{F}^0_{nm}$, and thus the total force $\mathbf{F}^0_m$ on an ion

TABLE VIII. Comparison of experimental and theoretical surface structures for Al(210).

	Experiment		Theory		
	Present work	Barnett *et al.*	Jiang *et al.*	Present work[a]	
x_n	Δx_n (%)	Δx_n (%)	Δx_n (%)	$F^0_n-F^0_{n+1}$	$F^{00}_n-F^{00}_{n+1}$
d_1	−15.5±2.4	−27.7	−19.3	−15.5	−12.5
d_2	−0.8±2.9	−10.2	−2.3	−3.0	−4.5
d_3	+8.9±2.6	+25.9	+4.8	+1.5	+1.8
d_4	−4.4±3.6	−12.8	−1.1	−0.3	−0.3
d_5	−1.2±4.6	−2.4	−0.8	+0.1	+0.1
r_1	−0.1±3.4	−2.5	+0.4	+1.9	+5.1
r_2	−3.2±3.1	−10.0	−8.5	−3.2	−5.1
r_3	+1.7±3.1	+3.8	+3.3	+1.9	+2.3
r_4	−2.0±4.0	−1.0	−0.3	−0.4	−0.4
r_5	−0.9±4.6	−2.0	−0.2	0.0	0.0

[a]The two final columns give the differences between the initial electrostatic forces on layers n and $n+1$ of the unrelaxed surface, as calculated using the point-ion–frozen-background model. The forces F^0_n and F^{00}_n are multiplied by $67.8\,A/4\pi Z^2$, see Sec. VIII C.

in the mth net is obtained as the (geometric) sum over the contributions from all other layers as

$$F_m^0(z)=\frac{4\pi Z^2}{A}\sum_{\mathbf{g}}{}''\,\mathrm{Re}(f_m^0)\ ,$$

$$F_m^0(x)=\frac{4\pi Z^2}{A}\sum_{\mathbf{g}}{}''\,\mathrm{Im}\left[\frac{g_x}{g}f_m^0\right]\ , \tag{8.4}$$

where

$$f_m^0=e^{-mgd}e^{-im\mathbf{g}\cdot\mathbf{v}}/(1-e^{-gd}e^{-i\mathbf{g}\cdot\mathbf{v}})\ .$$

A number of simple deductions can be made from Eqs. (8.3) and (8.4), but their usefulness can only be gauged by first examining the extent to which the calculated forces lead to a correct prediction of the trends of multilayer relaxation. We have therefore used Eq. (8.4) to calculate the initial forces on the unrelaxed structures of the six most close-packed bcc and fcc surfaces. These results will be described in detail elsewhere,[59] but we note here that consideration of the initial forces leads in almost all cases to the prediction of the same relaxation sequences as those determined by Jiang *et al.*[57,58] by minimization of the surface energy. This is illustrated for Al(210) by the results listed in the last two columns of Table VIII, where the differences $\mathbf{F}_n^0-F_{n+1}^0$ and $\mathbf{F}_n^{00}-\mathbf{F}_{n+1}^{00}$ (see below) are compared to the relaxations Δd_n and Δr_n of the interlayer spacings and registries. For the sake of this comparison we assume that the relaxations are linearly proportional to the initial forces in the limit of small relaxations. In Table VIII the forces $\mathbf{F}_n^0$ and $\mathbf{F}_n^{00}$ have been arbitrarily multiplied by $67.8(A/4\pi Z^2)$ to give numerical agreement between the experimental value of Δd_1 and the value of $F_1^0(z)-F_2^0(z)$. It can be seen from the results given in Table VIII that consideration of the initial forces leads to the same qualitative relaxation sequence as given by the calculations of Jiang *et al.*, for the first four interlayer spacings and registries.

Based on these results, and results[59] for other surfaces of Al and Fe we believe that Eq. (8.4) provides a useful, almost back-of-the-envelope method for prediction of relaxation trends. (The calculations take a few seconds on a personal computer or a few minutes on a programmable calculator.) In the context of the present discussion, however, it is of equal interest to enumerate some of the simple physical consequences of Eqs. (8.3) and (8.4), some of which apply also when the equations are generalized to the case of nonvanishing relaxations.

Firstly, we note that it follows simply from Eq. (8.4) that for surfaces with a mirror plane, say the xz plane, the forces (and hence relaxations) are contained within the mirror plane, since

$$e^{-i\mathbf{g}\cdot\mathbf{v}}=e^{-i\mathbf{g}^m\cdot\mathbf{v}}$$

but

$$g_y=-g_y^m\ ,$$

where $\mathbf{g}$ and $\mathbf{g}^m$ are connected by a mirror operation, and thus $F_m^0(y)=0$.

Secondly, as noted previously, it follows from Eq. (8.3) that $\mathbf{F}_{mn}=-\mathbf{F}_{nm}$. Thus the contributions of layers 1 to $m-1$ to the total force on an ion in net m are cancelled by the contributions of layers $m+1$ to $2m-1$, such that the first effective contribution comes from layer $2m$. This accounts for the factor e^{-mgd} in Eq. (8.4) which leads to an overall exponential decay of the forces (and relaxations) with depth.

Thirdly, it is evident that the signs of the force components on a given layer are governed by the phase factors $e^{-im\mathbf{g}\cdot\mathbf{v}}$. For a surface with a bulk repeat period of p layers, where $e^{-ip\mathbf{g}\cdot\mathbf{v}}=1$, it follows that $e^{-im\mathbf{g}\cdot\mathbf{v}}=e^{i(m+p)\mathbf{g}\cdot\mathbf{v}}$, and thus that the signs of the forces are periodic with periodicity p layers.

Fourthly, since the contribution of successively deeper layers to the force on an ion in layer m falls roughly exponentially with depth, the signs of the forces are given

TABLE IX. Experimental interlayer relaxation of Al and Fe surfaces.

	Relaxations (%)				Missing nearest neighbors		
Surface	Δd_1	Δd_2	Δd_3	Δd_4	First layer	Second layer	Third layer
Al(111)	+1				3		
Fe(110)	+0.5				2		
Al(100)	~0				4		
Fe(100)	−5	+5			4		
Al(110)	−9	+5	−2		5	1	
Fe(211)	−10	+5	−1		3	1	
Al(311)	−13	+9			5	2	
Fe(310)	−16	+13	−4		4	2	
Al(331)	−12	−4	+10	−5	5	3	1
Fe(111)	−17	−10	+4	−2	4	1	1
Al(210)	−16	−1	+9	−4	6	3	1
Fe(210)	−22	−11	+17	−5	4	2	2

correctly by the approximations

$$F_m^{00}(z) \cong F_{m,2m}^0(z) = \frac{4\pi Z^2}{A} \sum_{\mathbf{g}}'' \mathrm{Re}(f_m^{00}) ,$$
$$F_m^{00}(x) \cong F_{m,2m}^0(x) = \frac{4\pi Z^2}{A} \sum_{\mathbf{g}}'' \mathrm{Im}\left[\frac{g_x}{g} f_m^{00}\right] , \quad (8.5)$$

where

$$f_m^{00} = e^{-mgd} e^{-im\mathbf{g}\cdot\mathbf{v}} .$$

The results in the final column of Table VIII were obtained using Eq. (8.5).

Thus, for example, the total force on the second layer is given approximately by the contribution of the fourth layer only, since the contributions from the first and third layers exactly cancel. For surfaces with a two-layer repeat period, it follows that $F_2(z)$ is positive, accounting for the observed outward movements of the second layers of Fe(100) and Al(110). $F_m(x)$ and $F_m(y)$ are always zero for these surfaces, of course, due to the existence of two orthogonal mirror planes.

More generally, evaluation of the signs of the force components on the mth layer of an arbitrary surface involves carrying out the summations over $\mathbf{g}$. However, for the surfaces considered here, the correct signs are obtained by inclusion of only the first one or two pairs of reciprocal-net vectors. Thus for fcc (210), where with the choice of unit-mesh vectors and $\mathbf{s}$ defined in Fig. 1, $\mathbf{g}_{hk}\cdot\mathbf{v} = (\pi/5)(7h+4k)$ and $g_{hk}d = (\sqrt{2}\pi/5)(3h^2+2k^2+2hk)^{1/2}$, the correct signs of all $F_m^0(z)$ and $F_m^0(x)$ for $m=1$ to 10 are obtained by inclusion of the (h,k) pairs $(0,\pm1)$ and $(\pm1,0)$ only.

To summarize, we have shown that the qualitative trends of the multilayer relaxation of open metal surfaces can be predicted simply by calculating the electrostatic forces on the layers of the unrelaxed structures, and that the nature of the trends can be understood in simple physical terms. We confess, nevertheless, that consideration of the interactions between infinite nets of ions has for us a less-immediate intuitive appeal than considerations based on the number and configuration of nearest neighbors. We believe, therefore, that an examination of the Hellman-Feynman forces on atoms of the unrelaxed structure within the framework of the effective-medium model might prove to be illuminating.

*Permanent address: Hefei Polytechnical University, Hefei, Anhui, People's Republic of China.

[1]R. N. Barnett, U. Landman, and C. L. Cleveland, Phys. Rev. Lett. **51**, 1359 (1983).
[2]H. L. Davis and J. R. Noonan, Phys. Rev. Lett. **54**, 566 (1985).
[3]W. Moritz and D. Wolf, Surf. Sci. **163**, L655 (1985).
[4]R. Baudoing, Y. Gauthier, and Y. Joly, J. Phys. C **18**, 4061 (1985).
[5]D. W. Jepsen, P. M. Marcus, and F. Jona, Phys. Rev. B **6**, 3684 (1972); **5**, 3933 (1972); **8**, 1786 (1973); Surf. Sci. **31**, 180 (1972).
[6]D. P. Jackson, Can. J. Phys. **49**, 2093 (1971).
[7]L. Kleinman, Phys. Rev. **3**, 3083 (1971); M. W. Finnis and V. Heine, J. Phys. F **4**, L37 (1974).
[8]G. P. Alldredge and L. Kleinman, Phys. Lett. **48A**, 37 (1974); J. Phys. F **4**, L207 (1974).
[9]N. D. Lang and W. Kohn, Phys. Rev. B **1**, 4555 (1970).
[10]J. N. Andersen, H. B. Nielsen, L. Petersen, and D. L. Adams, J. Phys. C **17**, 173 (1984).
[11]J. R. Noonan, H. L. Davis, and L. H. Jenkins, J. Vac. Sci. Technol. **15**, 619 (1978).
[12]H. L. Davis, J. R. Noonan, and L. H. Jenkins, Surf. Sci. **83**, 559 (1979).
[13]J. R. Noonan and H. L. Davis, Surf. Sci. **99**, L424 (1980).
[14]U. Landman, R. N. Hill, and M. Mostoller, Phys. Rev. B **21**, 448 (1980).
[15]D. L. Adams, H. B. Nielsen, J. N. Andersen, I. Stensgaard, R. Feidenhans'l, and J. E. Sørensen, Phys. Rev. Lett. **49**, 669 (1982).
[16]I. Stensgaard, R. Feidenhans'l, and J. E. Sørensen, Surf. Sci. **128**, 281 (1983).
[17]D. L. Adams, H. B. Nielsen, and J. N. Andersen, Surf. Sci. **128**, 294 (1983).
[18]H. B. Nielsen, J. N. Andersen, L. Petersen, and D. L. Adams, J. Phys. C **15**, L1113 (1982).
[19]H. L. Davis and J. R. Noonan, Surf. Sci. **126**, 245 (1983).
[20]J. R. Noonan and H. L. Davis, Phys. Rev. B **29**, 4349 (1984).
[21]M. Copel, T. Gustafsson, W. R. Graham, and S. M. Yalisove, Phys. Rev. B **33**, 8110 (1986).
[22]R. N. Barnett, U. Landman, and C. L. Cleveland, Phys. Rev. B **27**, 6534 (1983).
[23]C. L. Fu, S. Ohnishi, H. J. F. Jansen, and A. J. Freeman, Phys. Rev. B **31**, 1168 (1985).
[24]K. M. Ho and K. P. Bohnen, Phys. Rev. B **2**, 3446 (1985).
[25]V. Jensen, J. N. Andersen, H. B. Nielsen, and D. L. Adams, Surf. Sci. **116**, 66 (1982).
[26]A. Titov and W. Moritz, Surf. Sci. **123**, L709 (1982).
[27]R. Feidenhans'l, J. E. Sørensen, and I. Stensgaard, Surf. Sci. **134**, 329 (1983).
[28]Y. Gauthier, R. Baudoing, Y. Joly, C. Gaubert, and J. Rundgren, J. Phys. C **17**, 4547 (1984).
[29]D. L. Adams, L. E. Petersen, and C. S. Sørensen, J. Phys. C **18**, 1753 (1985).
[30]M. L. Xu and S. Y. Tong, Phys. Rev. B **31**, 6332 (1985).
[31]S. M. Yalisove, W. R. Graham, E. D. Adams, M. Copel, and T. Gustafsson, Surf. Sci. **171**, 400 (1986).
[32]H. L. Davis and J. R. Noonan, in Ref. 19.
[33]Y. Kuk and L. C. Feldman, Phys. Rev. B **30**, 5811 (1984).
[34]J. W. M. Frenken, J. V. van der Veen, R. N. Barnett, U. Landman, and C. L. Cleveland, Surf. Sci. **172**, 319 (1986).
[35]C. J. Barnes, M. Q. Ding, M. Lindroos, R. D. Diehl, and D. A. King, Surf. Sci. **162**, 59 (1985).
[36]D. L. Adams, W. T. Moore, and K. A. R. Mitchell, Surf. Sci. **149**, 407 (1985).
[37]J. R. Noonan, H. L. Davis, and W. Erley, Surf. Sci. **152**, 142 (1985).
[38]J. Sokolov, H. D. Shih, U. Bardi, F. Jona, and P. M. Marcus, Solid State Commun. **48** 739 (1983); J. Phys. C **17**, 371 (1984).
[39]J. Sokolov, F. Jona, and P. M. Marcus, Phys. Rev. B **29**, 5402 (1984).
[40]J. Sokolov, F. Jona, and P. M. Marcus, Phys. Rev. B **33**, 1397

(1986).
[41]J. Sokolov, F. Jona, and P. M. Marcus, Phys. Rev. B **31**, 1928 (1984).
[42]D. L. Adams and C. S. Sørensen, Surf. Sci. **166**, 495 (1986).
[43]J. F. Nicholas, *An Atlas of Models of Crystal Structures* (Gordon and Breach, New York, 1965).
[44]A. Taylor and B. J. Kagle, *Crystallographic Data on Metal and Alloy Structures* (Dover, New York, 1963).
[45]D. F. Gibbons, Phys. Rev. **112**, 136 (1958).
[46]J. B. Pendry, *Low Energy Electron Diffraction* (Academic, London, 1974).
[47]M. A. Van Hove and S. Y. Tong, *Surface Crystallography by LEED* (Springer-Verlag, Berlin, 1979).
[48]D. L. Adams, J. Phys. C **16**, 6101 (1983).
[49]V. L. Moruzzi, J. F. Janak, and A. R. Williams, *Calculated Electronic Properties of Metals* (Pergamon, New York, 1978).
[50]J. Rundgren and A. Salwen, J. Phys. C **7**, 4247 (1974); **9**, 3701 (1976).
[51]M. A. Van Hove and J. B. Pendry, J. Phys. C **8**, 1362 (1975).
[52]D. L. Adams, H. B. Nielsen, and M. A. Van Hove, Phys. Rev. B **15**, 4789 (1979).
[53]D. W. J. Cruickshank, in *International Tables for X-Ray Crystallography* (Kynoch, Birmingham, 1972), Vol. II, p. 84.
[54]J. R. Noonan and H. L. Davis, in *Determination of Surface Structure by LEED*, edited by P. M. Marcus and F. Jona (Plenum, New York, 1984).
[55]E. Zanazzi and F. Jona, Surf. Sci. **62**, 61 (1977).
[56]J. B. Pendry, J. Phys. C **13**, 937 (1980).
[57]F. Jona (private communication).
[58]P. Jiang, P. M. Marcus, and F. Jona, Solid State Commun. **59**, 275 (1986).
[59]D. L. Adams (unpublished).
[60]S. P. Chen, A. F. Voter, and D. J. Srolovitz, Phys. Rev. Lett. **57**, 1308 (1986).
[61]M. S. Daw and M. I. Baskes, Phys. Rev. B **29**, 6443 (1984).
[62]F. Jona, D. Sondericker, and P. Marcus, J. Phys. C **13**, L155 (1980).
[63]H. B. Nielsen and D. L. Adams, J. Phys. C **15**, 615 (1982).
[64]K. W. Jacobsen, J. K. Nørskov, and M. J. Puska, Phys. Rev. B **35**, 7423 (1987).
[65]M. P. Tosi, in *Solid State Physics*, edited by F. Seitz, D. Turnbull, and H. Ehrenreich (Academic, New York, 1964), Vol. 16, Eq. (B19).